EPJ Web of Conferences **26**, 03001 (2012)
DOI: 10.1051/epjconf/20122603001


# Determination of dynamic material properties for poly(L-lactic acid)/poly($\epsilon$-caprolactone) blends: Experiments and simulation using split Hopkinson pressure bars

M. Nishida[1,a], Y. Ito[1], G. Gustafsson[2], H.-Å. Häggblad[2], P. Jonsén[2], and T. Takayama[3], and M. Todo[4]

[1] *Nagoya Institute of Technology, Gokiso-cho, Showa-ku, Aichi 466-8555, Japan*
[2] *Luleå University of Technology, 97187 Luleå, Sweden*
[3] *Yamagata University, 4-3-16 Jonan, Yonezawa, Yamagata 992-8510, Japan*
[4] *Kyushu University, 6-1 Kasuga-koen, Kasuga, Fukuoka 816-8580, Japan*

**Abstract.** Coefficients of Cowper-Symonds constitutive equation for PLLA/PCL = 80/20 were determined using the results of compressive tests at high and low strain rates. The simulation of split Hopkinson pressure bar using the coefficients was carried out under the same condition as the experiments. The diameter and thickness of specimens were measured by a high-speed video camera. The stress and strain histories of specimens, the thickness and the diameter in the simulations at high strain rate were compared with those in the experiments.

## 1 Introduction

Poly(L-lactic acid) (PLLA) shows good biocompatibility and is decomposed and absorbed within living organisms. PLLA is widely used for bone fixation devices which do not require second surgery for removal in the fields of orthopedics and oral surgery. In order to overcome the brittleness and low impact strength of PLLA, its mechanical properties have been improved by blending with ductile polymers or natural fiber reinforcing. Since Poly($\epsilon$-caprolactone) (PCL) is a ductile, bioabsorbable polymer, many types of PLLA/PCL polymer blends have been developed to improve its material strength and impact resistance [1–5]. Although good results have been reported, in most cases, the impact resistances of PLLA/PCL polymer blends are based only on the experimental results of Izod impact strength tests or Charpy impact strength tests. The basic mechanical properties of these polymer blends with respect to impact resistances are still unknown. Also, these mechanical properties have not yet been fully elucidated at higher strain rates.

The authors have been studying the strain rate dependence of PLLA/PCL polymer blend specimens [6]. In the present study, the specimens of PLLA and PCL polymer blends which mixing ratio (mass fraction) was 80:20 were used. (For details of specimens, please see [6]) X-ray computed tomography (Shimadzu, inspeXio SMX-225CT) of specimen was shown in Fig. 1. It shows a homogeneous density distribution. Coefficients of Cowper-Symonds constitutive equation for PLLA/PCL = 80/20 were determined using the results of compressive tests at high and low strain rates. The simulation of split Hopkinson pressure bar (Kolsky bar) using the coefficients was carried out under the same condition as the experiments. The stress and strain histories of specimens, the thickness and the diameter in the simulations at high strain rate were compared with those in the experiments.

[a] e-mail: nishida.masahiro@nitech.ac.jp

## 2 SHPB model

### 2.1 Experimental methods

At high strain rates of $10^2$ to $10^3\,s^{-1}$, the stress-strain curves of the PLLA/PCL = 80/20 were measured by the split Hopkinson pressure bar method, as shown in Fig. 2. The input and output bars were made of an aluminum alloy (A2024-T4), and they had a diameter of 28 mm and respective lengths of 1900 mm and 1300 mm. Strain gages were placed on the input and output bars at distances of 950 mm and 300 mm from the specimen, respectively. Because the stress histories were almost equal on both sides of the specimens, the stress and strain of the specimens were calculated from the strain on the bars using eqns. (1) and (2), which are given below [7,8].

$$\sigma_{av}(t) = \frac{AE}{A_s}\varepsilon_T(t) \tag{1}$$

$$\varepsilon_{av}(t) = \frac{2c_3}{L}\int_0^t [\varepsilon_I(t) - \varepsilon_T(t)]dt \tag{2}$$

Here, $\varepsilon_I$ and $\varepsilon_T$ denote the axial strains induced in the input bar by the incident wave and in the output bar by the transmitted wave, respectively. $E$ and $c_3$ respectively denote the Young's modulus and elastic wave velocity of the input and output bars. $L$ denotes the specimen thickness. $A$ and $A_S$ denote the cross-sectional areas of the input/output bars and specimens, respectively. The material constants of the aluminum alloy (A2024-T4) bars used in the calculations are listed in Table 1. Brass strikers with a diameter of 20 mm and lengths of 220–390 mm were used. The specimens used for the dynamic tests had a

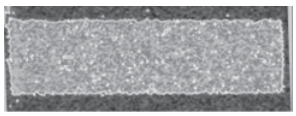

**Fig. 1.** X-ray computed tomography of specimen.

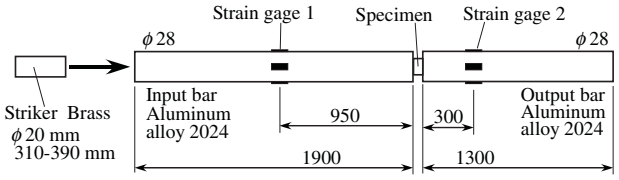


**Fig. 2.** Experimental setup for split Hopkinson pressure bar method.

**Table 1.** Material constants of input and output bars used in calculation.

| Density | Elastic wave velocity in bar, $c_3$ | Young's modulus, $E$ |
|---|---|---|
| $2.77 \times 10^3$ kg/m$^3$ | 5150 m/s | 73.6 GPa |

diameter of approximately 13 mm and a thickness of 4 mm to enable accurate measurement of the stress-strain curves using the equipment as shown in Fig. 2. The average value of the strain rate–train curve was used as the strain rate because the strain rate is not constant during compression.

Quasi-static compressive tests were conducted at strain rates ranging from $10^{-4}$ to $10^{-2}\,s^{-1}$ using a universal testing machine (A&D Co., Ltd., RTM-500). In the quasi-static compressive tests based on ASTM D695-02a, cylindrical specimens with a diameter and thickness of 6 mm and 9 mm, respectively, was used. The specimens immediately before dynamic and static compression were at a temperature of $25 \pm 2$°C. The specimens were preserved in a desiccator at a humidity of 30–40% until just before use in order to avoid being affected by moisture absorption. At low strain rate, the true stress-true strain curves were obtained by measuring the deformation of the gage area using a camera. Even at high strain rate, it was reported that the incompressibility (constancy of volume) of polycarbonate can be approximately satisfied when the strain is greater than the yield strain (i.e. Siviour et al. [9] and Lu and Li [10]). The following equations were used.

$$\sigma^T_{av}(t) = \sigma_{av}(1 - 0.5\,\varepsilon_{av})^2 \tag{3}$$

$$\varepsilon^T_{av}(t) = -\ln(1 - \varepsilon_{av}) \tag{4}$$

The incompressibility of PLLA/PCL polymer blends has not been fully revealed. Here, it was assumed that, at high strain rate, the incompressibility of this material can be approximately satisfied, in other words, Poisson's ratio is 0.5, during compression and eqs. (3) and (4) were used. The calculated volume of specimens after compression was almost the same as that before compression. The variation in the diameter and thickness of specimens

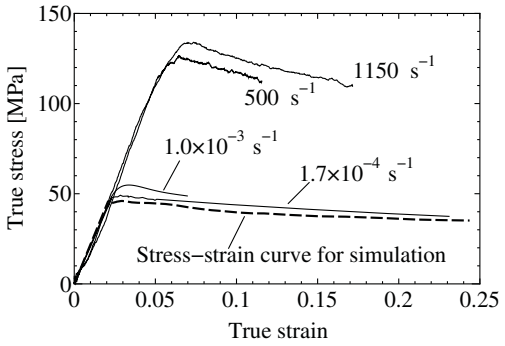


**Fig. 3.** True stress – true strain curves for PLLA/PCL = 80/20.

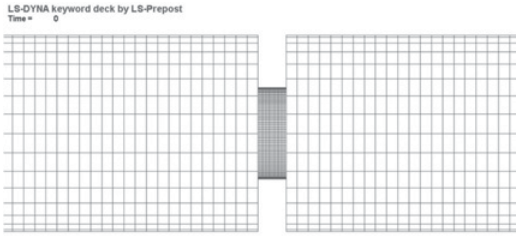


**Fig. 4.** Simulation model for split Hopkinson pressure bar method.

were measured by a high-speed video camera (Photron, FASTCAM-1024PCI).

### 2.2 FEM simulation

For the numerical computations and analyses, the commercial nonlinear finite element code LS-Dyna v971 R5.1 [11] has been used for the modeling and simulation of SHPB. The SHPB in simulation consists of input bar, output bar and specimens. Instead of modeling striker in the simulation, initial velocity with an adjusted amplitude and a adjusted duration was applied to the left end of the input bar so as that the incident wave in the simulation becomes almost the same as that in the experiment. A three-dimensional model with eight-node hexahedral solid elements and the explicit solver were applied for SHPB simulation. Here, the input bar and output bar were modeled as a linear elastic material. The specimen were assumed as an elasto-plastic material model that takes into account the strain rate dependency of Cowper-Symonds type [12];

$$\frac{\sigma_y}{\sigma_s} = 1 + \left(\frac{\dot{\varepsilon}}{C}\right)^{(1/p)} \tag{5}$$

Here, $\sigma_y$ and $\sigma_s$ denote the dynamic flow stress at a uniaxial plastic strain rate, $\dot{\varepsilon}$, and the associated static flow stress, respectively. $C$ and $p$ are constants for a material. Even though the yield surface of polymers is often affected by the hydrostatic stress components, the pressure-dependent model was not used in this simulation. The true stress-true strain curve drawn by a dashed line in Fig. 3 was used as the static true stress-strain curve of the specimen. The specimens were meshed into 32 elements in the radial direction and 22 elements in the axial direction as shown in Fig. 4. To calculate accurately the stress-strain relation, small elements are needed in the modeling of the

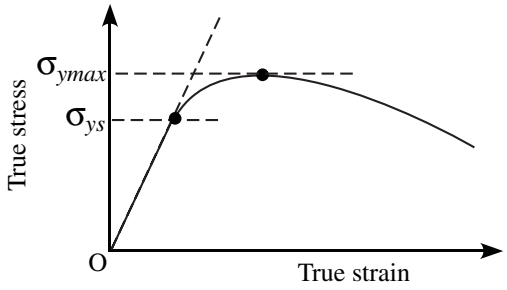


**Fig. 5.** Definition of stress at plastic deformation onset and maximum stress.

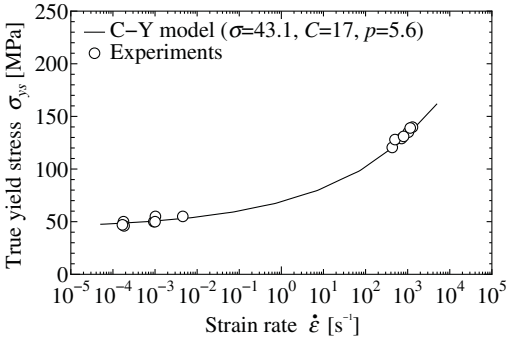


**Fig. 6.** Strain rate dependency of stress at yield onset.

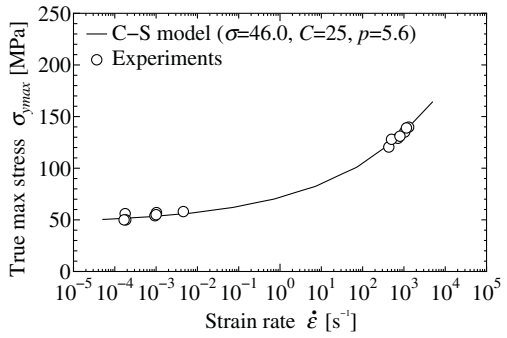


**Fig. 7.** Strain rate dependency of maximum yield stress.

specimens and bars. The input bar and output bar were represented 11 elements in the radial direction and 1187 and 811 elements in the axial directions. The sliding is permitted between the specimen and the bars. The contact between bars and specimen was assumed frictionless.

## 3 Results and discussion

The true stress-true strain curves for PLLA/PCL = 80/20 are shown in Fig. 3. The flow stress increased with increasing strain rate as expected. Regardless of strain rate, Young's modulus was approximately 2.3 GPa. The stress at plastic deformation onset $\sigma_{ys}$ and the maximum stress $\sigma_{ymax}$, was defined as shown in Fig. 5, in order to examine the strain rate dependency of yield stress. The strain rate dependencies of the yield stresses $\sigma_{ys}$ and $\sigma_{ymax}$ are shown in Figs. 6 and 7. By fitting the undetermined coefficients of Cowper-Symonds model to the experimental results, the values of these parameters for each yield stress were

**Table 2.** Coefficient of Cowper-Symonds equation for PLLA/PCL = 80/20.

| | $\sigma_s$ [MPa] | $C$[s$^1$] | $p$ |
|---|---|---|---|
| $\sigma_{ys}$ | 43.1 | 17 | 5.6 |
| $\sigma_{max}$ | 46.0 | 25 | 5.6 |
| Average value | | 21 | 5.6 |

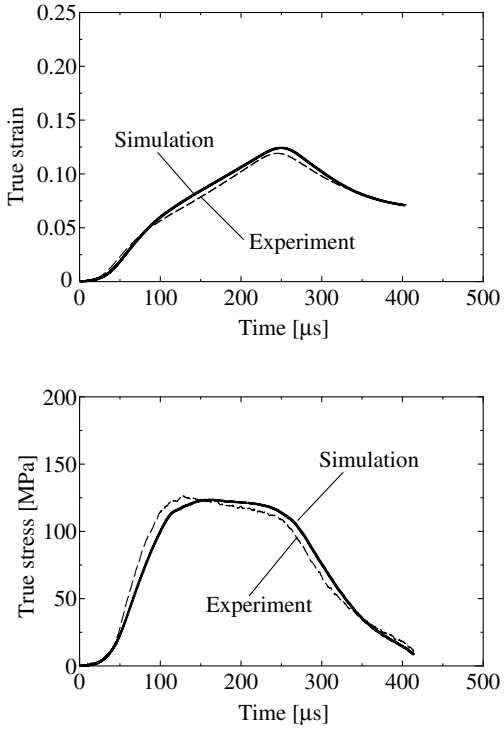


**Fig. 8.** Stress history and strain history at average strain rate of 550 [1/s].

obtained. Based on the values, $C = 81.96$, $p = 4.51$ for nylon [13], $C = 349.65$, $p = 5.494$ [14] and $C = 104.59$, $p = 6.72$ [15] for epoxy as an initial value, these coefficients were sought using trial-and-error method. The determined values are shown in Table 2. The average values of $C$ and $p$ are 21 s$^{-1}$ and 5.6, respectively.

The simulations using the values were carried out. In Figs. 8 and 9, the stress histories and strain histories of specimen in the simulation were compared with those in the experiments. The stress histories and strain histories of specimen in the simulation were also calculated using eqs. (1) and (2) and the strain histories on the bar in the simulation. The method to obtain the stress and strain of specimens is the same between in the experiment and simulation. Therefore, the difference in the results between simulations and experiments did not include the difference in the calculation method. In Figs. 8(a) and 9(a), the strain histories in the simulation were almost the same as those in the experiment other than the unloading parts. In Figs. 8(b) and 9(b), the softening behavior after showing the maximum stress and the values of the maximum stress were almost the same. The initial slope in the simulation was steeper than that in the experiments. It is highly

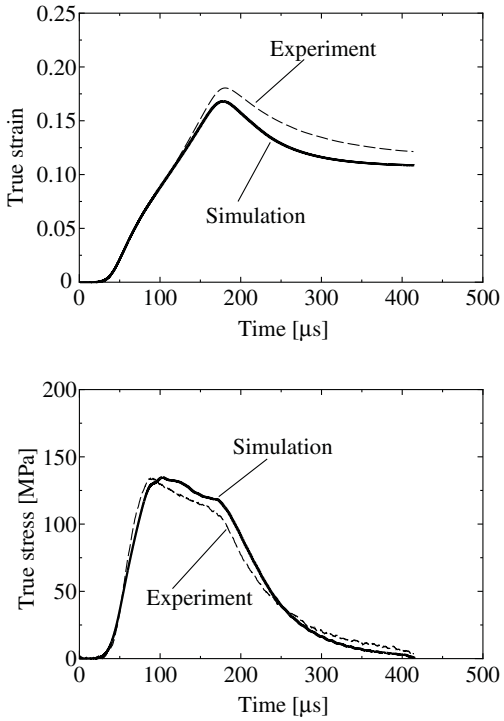


**Fig. 9.** Stress history and strain history at average strain rate of 1150 [1/s].

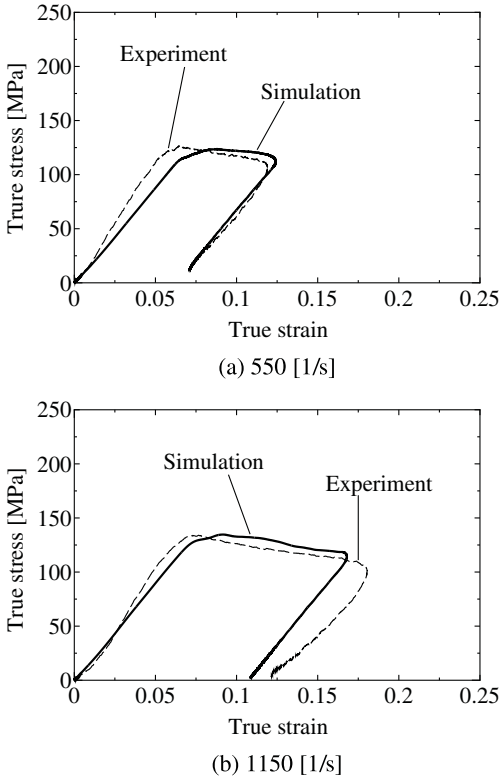


**Fig. 10.** Comparison of stress-strain curves between simulation and experiment.

possible that the viscosity of materials was important in this region, because the slope of unloading process was not the same as the initial slope as shown in Fig. 10. The thickness measured immediately after compression was almost the same as the thickness measured 7 days later.

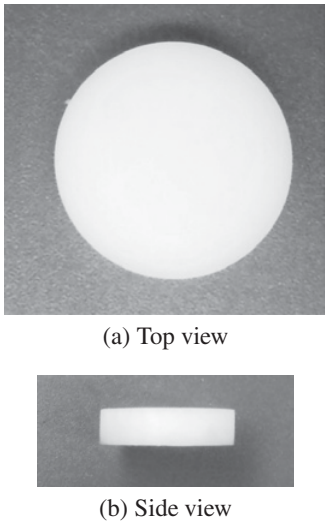

(a) Top view

(b) Side view

**Fig. 11.** Photograph of compressive test specimen after compression (Experiment); 550 [1/s] of Fig. 7.

**Table 3.** Comparison of diameter between before and after compression.

| | | Diameter | | |
|---|---|---|---|---|
| | | Before compression | After compression | Variation |
| $550\,s^{-1}$ | Experiment | 13.15 mm | 13.45 nm | +2.3% |
| | Simulation | 13.00 mm | 13.43 mm | +3.3% |
| $1150\,s^{-1}$ | Experiment | 13.00 mm | 13.60 mm | +4.6% |
| | Simulation | 13.00 mm | 13.73 mm | +5.6% |

It seems that the viscosity of this material is not high. However, the main reason for this is still unclear, and more detailed investigation is required.

The ratios of the measured thickness and diameter to the initial thickness and diameter are shown in Fig. 12. Because the images of specimen were taken with a resolution of 128 × 208 pixels using a high speed video camera, the measurement error of thickness and diameter is approximately 0.087 mm/pixel (0.022 in Fig. 12). The variation of thickness and diameter could be roughly simulated by this simulation model. The final thickness and final diameter of specimen were also compared in Table 3. Even though the simulation slightly overestimated the final thickness and final diameter, the final thickness and final diameter in the simulation were almost the same as those in the experiments. Figures 11(a) and (b) show photographs of a specimen after compression in the experiment. Figures 13(a) and (b) show specimen shapes after compression in the simulation. The specimen flattens uniformly and the diameters of upper and lower sides were almost the same. Figures 14(a) and (b) show photographs of the cryo-fracture surfaces before and after compression. The same structures consisting of the PLA matrix and PCL particles (1–2 $\mu$m in diameter) were observed. The specimen after compression also did not have the distinctive feature that reflects plastic deformation.

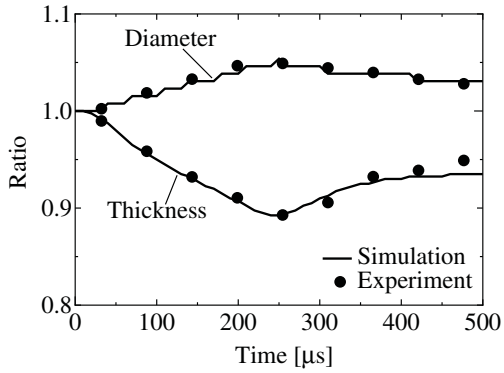


(a) 550 [1/s]

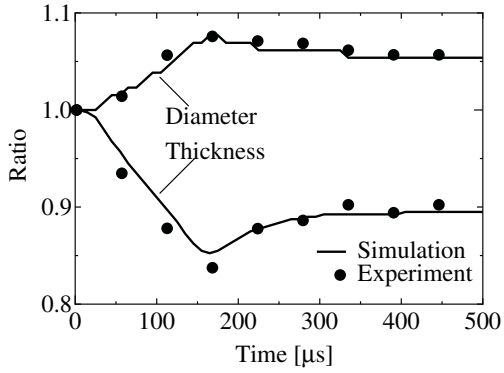


(b) 1150 [1/s]

**Fig. 12.** Comparison of thickness histories and diameter histories.

**Table 4.** Comparison of thickness between before and after compression.

| | | Thickness | | |
|---|---|---|---|---|
| | | Before compression | After compression | Variation |
| 550 $s^{-1}$ | Experiment | 3.90 mm | 3.75 nm | −3.8% |
| | Simulation | 4.00 mm | 3.74 mm | −6.5% |
| 1150 $s^{-1}$ | Experiment | 3.91 mm | 3.61 mm | −7.7% |
| | Simulation | 4.00 mm | 3.58 mm | −10.5% |

## 4 Conclusions

Strain rate dependence of a PLLA/PCL polymer blend has been presented numerically and experimentally. The validity of dynamic material properties determined using the experimental results of compressive tests are shown. Identification of the material properties and a general representation of the material behavior were found with acceptable predictability over the tested range of strain rates.

## Acknowledgements

The authors are greatly indebted to Dr. Fumihiro Itoigawa of Nagoya Institute of Technology for his help with taking images using a high speed camera.

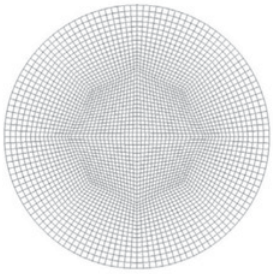

(a) Top view

(b) Side view

**Fig. 13.** Compressive test specimen after compression (Simulation); 550 [1/s] of Fig. 7.

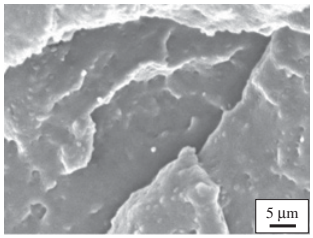


(a) Before compression

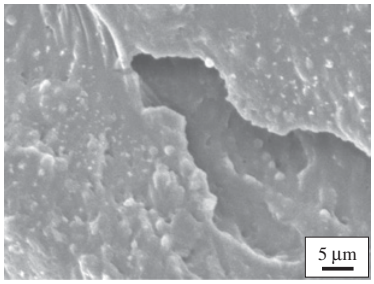


(b) After compression

**Fig. 14.** Photographs of cryo-fractured surfaces taken using a scanning electron microscope; 1150 [1/s] of Fig. 8.

## References

1. H. Tsuji, Y. Ikeda, J. Appl. Polym. Sci., **70** (1996), pp. 2367-2375
2. C.C. Chen, J.Y. Chueh, H. Tseng, H.M. Huang, S.Y. Lee, Biomaterials, **24** (2003), pp. 1167-1173
3. T. Takayama and M. Todo, J. Mater. Sci., **41** (2006) pp. 4989-4992
4. M. Todo, S.-D. Park, T. Takayama, K. Arakawa, Eng. Fract, Mech., **74** (2007), pp. 1872-1883
5. T. Takayama, M. Todo, H. Tsuji, J. Mech. Behav. Biomed. Mater. **4**, (2011) 255-260
6. M. Nishida, M. Yamaguchi, M. Todo, T. Takayama, H.-Å. Hagğblad and P. Jonsén, *Proceedings of DYMAT 2009* (EDP Science, 2009) pp. 909-915

7. G.T. Gray III, *Classic Split Hopkinson Pressure Bar Testing*, ASM Handbook, 8, Mechanical Testing and Evaluation, ASM., (2000) 462-476.
8. W. Chen, B. Song, *Split Hopkinson (Kolsky) Bar: Design, Testing and Applications* (Springer, 2010)
9. C.R. Siviour, S.M. Valley, W.G. Proud, J.E. Field, Polymer, **46** (2005), pp. 12546-12555.
10. Y.B. Lu, Q.M. Li, Int. J. Impact Eng., **38** (2011), pp. 41-50.
11. LS-DYNA, Keyword user's manual, vol. 1 (2007) version 971.
12. G.R. Cowper, P.S. Symonds, Brown University Division of Applied Mathematics Report No. 28, September (1957).
13. R.T. Moura, L.M. Mazzariol, A.H. Clausen, M. Langseth, M. Alves, *Proceedings of the IMPLAST 2010 Conference* (SEM, 2010).
14. I.G. Grouch, L.J. Greaves, C. Ruiz, J. Harding, J. Physique IV, **4** C8 (1994), pp. C8-201-206.
15. T. Nagai, T. Iwamoto, T. Sawa, Y. Sekiguchi, Int J Mod Phys B, **22** 31-32 (2008), pp. 5590-5595.